Article

Not peer-reviewed version

Zircons from Eclogite-Associated Rocks of the Marun-Keu Complex, the Polar Urals: Trace Elements and U-pb Dating

Laysan Salimgaraeva *, Aleksey Berezin, Sergey Sergeev, Nikolai Gubanov, Ekaterina Stetskaya, Sergey Skublov

Posted Date: 7 June 2024

doi: 10.20944/preprints202406.0415.v1

Keywords: zircon; trace elements; rare earth elements; U-Pb zircon geochronology; eclogites; pegmatites; the Marun-Keu complex; the Polar Urals

Article

Zircons from Eclogite-Associated Rocks of the Marun-Keu Complex, the Polar Urals: Trace Elements and U-Pb Dating

Laysan Salimgaraeva [1,2,3,*], Aleksey Berezin [1,4], Sergey Sergeev [5], Nikolai Gubanov [2,6], Ekaterina Stetskaya [3] and Sergey Skublov [1,2,3]

1 Institute of Precambrian Geology and Geochronology, Russian Academy of Sciences, St. Petersburg 199034, Russia
2 The Zavaritsky Institute of Geology and Geochemistry, Ural Branch of the Russian Academy of Sciences, Ekaterinburg 620016, Russia
3 Empress Catherine II Saint-Petersburg Mining University, St. Petersburg 199106, Russia
4 Saint-Petersburg State University, St. Petersburg 199034, Russia
5 AP Karpinsky Russian Geological Research Institute, St. Petersburg 199106, Russia
6 V.S. Sobolev Institute of Geology and Mineralogy, Siberian Branch of the Russian Academy of Sciences, Novosibirsk 630090, Russia
* Correspondence: fluoritecaf2@mail.ru

Abstract: The Marun-Keu complex plays a significant role in understanding the geological evolution of the Ural orogen; however, it remains poorly understood. This study aims to provide insights into the complex's age, protolith composition, rock formation conditions, and its position in the region's history. The zircons from the host granitic gneisses are characterized by magmatic cores with an age of 470 Ma and metamorphic rims with an age of approximately 370 Ma. We suggest that the metamorphic rims were formed during eclogite metamorphism and that the metagranitoids hosting the eclogites experienced eclogite metamorphism simultaneously with the basic and ultrabasic rocks that are common in this area. Heterogeneous zircons were also isolated from the selvage of a pegmatite vein, in which four domains are distinguished, two to three of which can be identified within single grains, as follows: 1) igneous cores with an age of approximately 470 Ma and the geochemical characteristics of zircon crystallized in basic rocks; 2) zircons recrystallized during eclogite metamorphism with geochemical characteristics intermediate between those of the magmatic cores and true eclogitic zircon; 3) pegmatitic zircon, exhibiting the most sharply differentiated REE spectra of all four domains, characterized by a prominent positive Ce anomaly and a weakly expressed negative Eu anomaly; and 4) eclogitic zircon, observed in the form of veins and rims, superimposed in relation to the other three domains. The age of the latter three domains is within the error range and is estimated to be approximately 370 Ma. This indicates that the processes of eclogite metamorphism and the formation of pegmatites occurred at approximately the same time in the studied area.

Keywords: zircon; trace elements; rare earth elements; U-Pb zircon geochronology; eclogites; pegmatites; the Marun-Keu complex; the Polar Urals

1. Introduction

The Urals region is a classic example of a fold belt that has undergone a complete geodynamic evolution cycle and represents one of the most significant structural elements of the Eurasian continent [1]. Metamorphic complexes containing eclogites are extensively developed in this region and serve as important markers for understanding the geodynamic settings and reconstructing the history of these fold belts. The Urals contain globally renowned examples of eclogite-containing complexes, including the Maksyutov and Marun-Keu complexes [2].

 doi:10.20944/preprints202406.0415.v1

The Marun-Keu complex is a key study area for understanding the geological history of the Ural orogen. A significant contribution to the understanding of this complex was made by N.G. Udovkina through her monograph "Eclogites of the Polar Urals," published in 1971. This work was based on detailed geological and petrographic investigations conducted in 1956 and 1962 [3]. However, despite its tectonic significance, the Marun-Keu complex remains poorly studied due to its challenging accessibility and complex geological structure. The age of the complex, the nature of the eclogite protoliths, the rock formation conditions, and its position in the region's development history remain subjects of debate [4–9], etc.

In terms of the ages of the rocks forming this complex, two clusters of probable ages for eclogite metamorphism have been identified in the area: Mesoproterozoic [10,11] and Paleozoic [3,11–15]. However, there is limited data available regarding the age of the host rocks [3,11,13,14]. The Rb-Sr and Sm-Nd systems have yielded uncertain results with significant date scatter requiring further interpretation [10,12,13]. Although U-Pb dating studies have produced similar dates [14,15], these results lack analysis of zircon trace element composition and mineral inclusions, both of which are crucial for accurate geochronological interpretation [16–20]. Therefore, a comprehensive study of zircons from rocks associated with eclogites in the Marun-Keu complex is necessary to gain an improved understanding of the area's geological history.

2. Geological Setting and Sample Description

The Marun-Keu complex is a tectonic block located in the Urals region, measuring ~14 × 70 km. It is elongated in a roughly NE–SW direction and is confined to the zone west of the Main Uralian Fault (Figure 1). The complex is bounded to the west by metavolcanic rocks, local granite and diorite intrusions, and metasedimentary complexes of late Neoproterozoic to early Palaeozoic age. These rocks underwent low-grade metamorphism of greenschist facies or below [3,8]. These rocks belong to the Nyarovey series and represent a recumbent block beneath the Marun-Keu complex. To the east, the complex borders the Syum-Keu ophiolite massif and metagabbroids, which form the hanging wall of the Main Uralian Fault [3,8].

 doi:10.20944/preprints202406.0415.v1

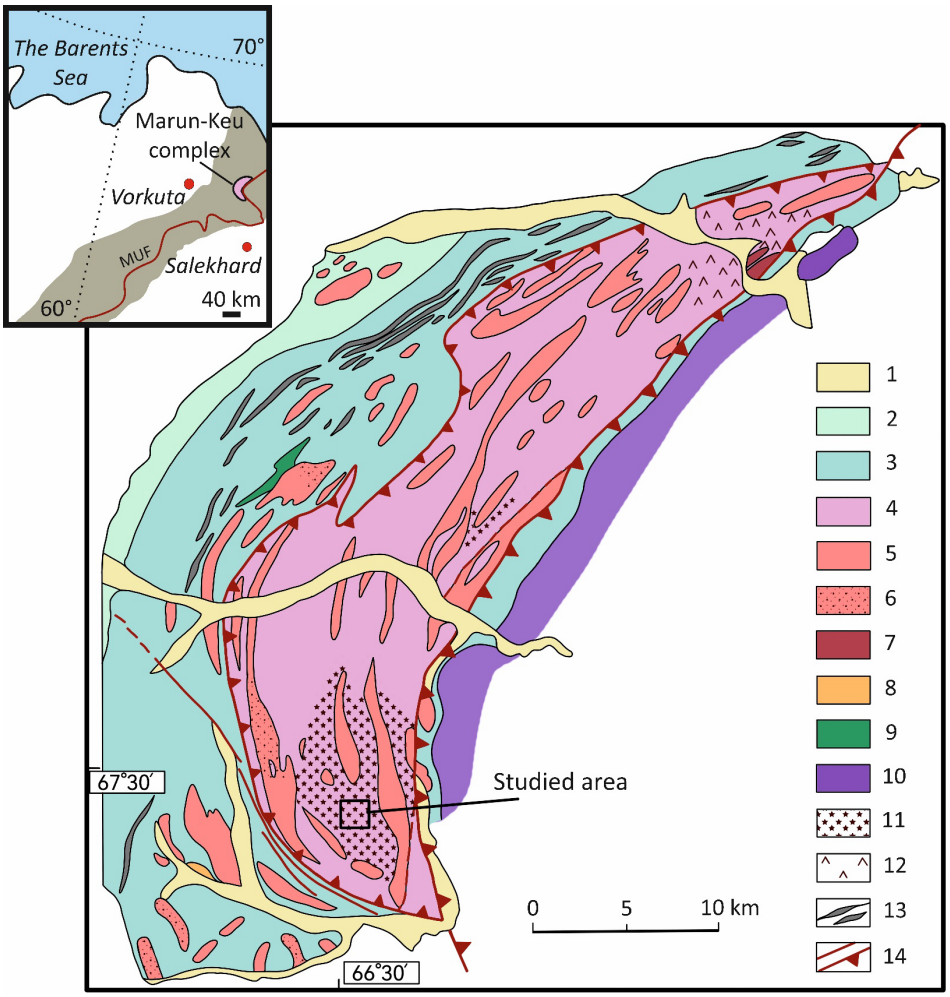

Figure 1. Geological map of the Marun-Keu complex [3]. The inset shows the overall geographic location of the Marun-Keu complex. MUF – Main Uralian Fault. Key: 1—Quaternary; 2— Ordovician (?); 3—greenschists of the Nyarovey formation; 4—Marun-Keu series: gneisses, eclogites; 5—gneisses, granite gneisses; 6—granites with fluorite; 7—meta-rhyolites; 8—diorites, 9—gabbroids; 10—ultramafic rocks (Syum-Keu complex); 11—predominately eclogites; 12—glaucophane; 13—quartz-graphite schists; 14—faults.

The southern part of the Marun-Keu complex, especially the area known as Mica Hill, contains the most complete eclogites and relics of their protoliths. Previous researchers [3-15, etc.] and the authors of the present study have primarily focused on this part of the complex. The eclogite outcrops are confined to the axial part of the Marun-Keu structure. The eclogites and their protoliths form lenticular blocks embedded in a granitic gneiss matrix. Three main groups of eclogite protoliths have been identified based on the authors' geological observations: peridotites, leucogabbros, and dolerite porphyrites, among which the peridotite-derived eclogites are the most common. The eclogite blocks and their associated rocks are elongated in a strip consistent with the strike direction of their host rocks; however, the primary contacts between these bodies have not yet been established. The orientations of linear elements within the eclogite blocks from different protoliths are not consistent. Combined with the above observations, this may imply the tectonic origin of these bodies. Based on geological observations, the age of the eclogites is interpreted to be the same as or older than that of their host rocks. The muscovite pegmatite veins observed cross-cutting the eclogite bodies provide a constraint for the latest possible date of eclogite formation.

This study focuses on an analysis of zircons derived from the host granitic gneisses and the selvage of a pegmatite vein within the peridotites. The samples were collected from an area called "the hill with peak 1040" (67° 28' 17" N, 66° 29' 24" E), which forms an elongated in a roughly NE–SW direction protrusion of ultramafic rocks measuring approximately 200 x 400 m (Figure 2a). This

 doi:10.20944/preprints202406.0415.v1

protrusion consists primarily of massive peridotites with a local shear zone containing eclogite lenses conformal to its orientation. This shear zone is around 10 m thick with a strike of 340° and a subvertical dip.

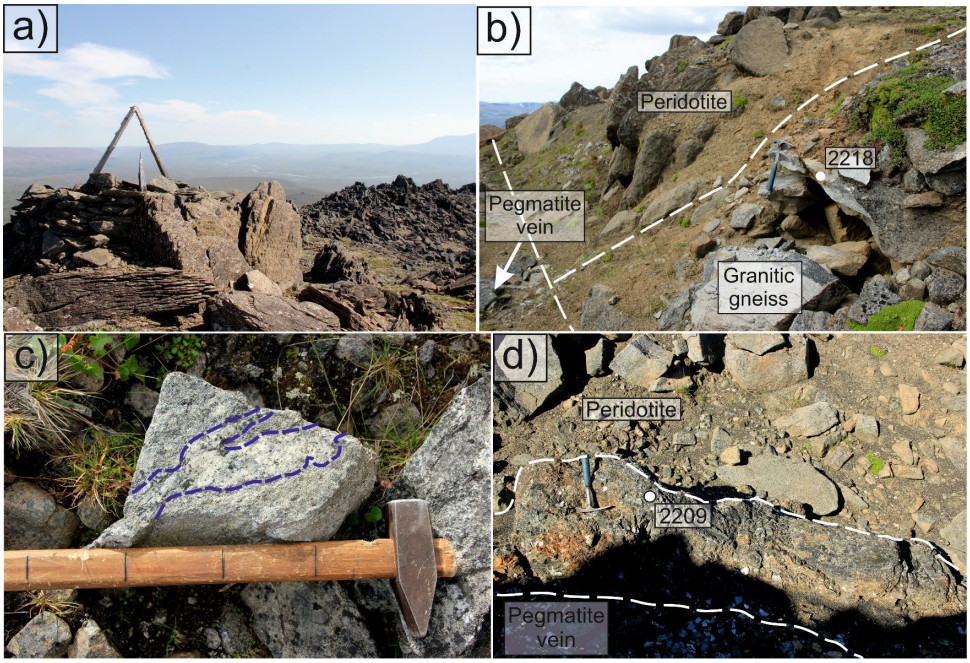

Figure 2. (a) General view of the peak 1040 area. **(b)** Contact between granitic gneisses and peridotites, crosscut by a 1.5 m wide pegmatite vein; white circle with sample number indicates the location from which sample 2218 was collected. The pegmatite vein was previously excavated for exploration purposes. **(c)** Migmatization zone in granitic gneisses indicated by a blue dashed line. **(d)** Selvage of a pegmatite vein at the contact with its host peridotites; white circle with sample number indicates the location from which sample 2209 was collected.

The granitic gneiss sample (2218) was collected from the southern foot of the hill in an exploration ditch in which a pegmatite vein was excavated (67° 28' 03" N, 66° 29' 20.5" E). This ditch cuts through both host rocks (granitic gneisses) and peridotites (Figure 2b). Isolated occurrences of migmatization are observed in the granitic gneisses (Figure 2c). The granitic gneiss is a fine-grained leucocratic rock with a weakly expressed directional schistose texture. The main rock-forming minerals are quartz, potassium feldspar, plagioclase, and micas. Epidote, apatite, rutile, and rare small garnet grains are present as accessory minerals (Figure 3a-d).

 doi:10.20944/preprints202406.0415.v1

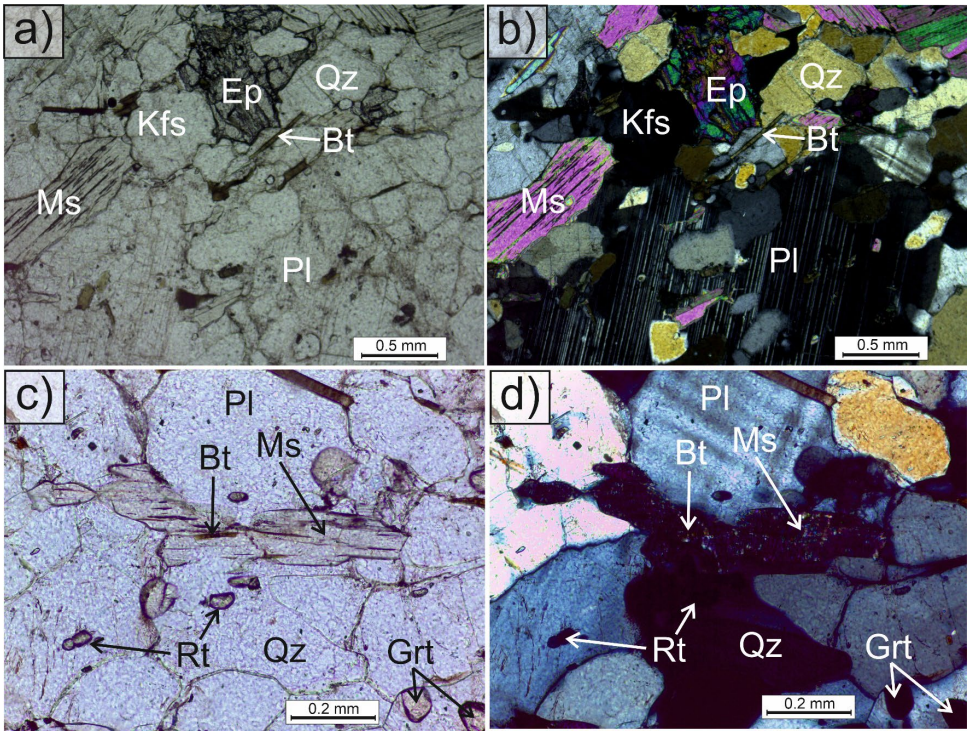

Figure 3. Microphotographs of thin section of granitic gneiss (sample 2218): **(a, c)** transmitted polarized light; **(b, d)** birefringence.

A sample from the selvage of a pegmatite vein (2209) was collected from a ditch on the eastern slope of the hill (67° 28' 16"N, 66° 29' 28.3"E). This ditch has a strike orientation of 275° and measures approximately 3x10 meters. The selvage material is a coarsely crystalline rock predominantly composed of muscovite and amphibole. The composition of the selvage is interpreted as host rock material (peridotite) that was reworked by fluids during pegmatite intrusion (Figure 2d).

3. Methods

Zircons were recovered from rocks using magnetic separation and heavy liquids. The recovered zircon grains were mounted in epoxy together with TEMORA [21] and 91500 [22] zircon standards. The spots for in situ analyses were selected based on both transmitted and reflected light images to avoid cracks and inclusions. Cathodoluminescence (CL) images were obtained at the Centre of Isotopic Research of the All-Russian Geological Research Institute (CIR). Back-scattered electron (BSE) images of the zircons were collected at the Institute of Precambrian Geology and Geochronology of Russian Academy of Sciences using a JEOL JSM-6510 LA scanning electron microscope with a JED-2200 (JEOL) energy dispersive system. The mineral abbreviations are given according to Warr [23].

U–Pb local dating was performed on the SIMS SHRIMP-IIe instrument at the Centre of Isotopic Research of the All-Russian Geological Research Institute using the method of given according to Williams [24], adopted for CIR according to Schuth et al. [25]. The intensity of the primary O_2 beam was 4 nA, and the analytical crater was 20 μm wide and 2 μm deep. The data obtained were processed using the SQUID program, according to Ludwig [26]. Differential fractionation between U and Pb was monitored using a reference Pb/U ratio of 0.0668 for the TEMORA standard zircon (416.8±0.3 Ma), according to Black et al. [27], based on the logarithmic law relationship of $^{206}Pb^+/U^+$ versus UO^+/U^+. The 91500 standard zircon with a uranium content of 81.2 ppm and a $^{206}Pb/^{238}U$ age of 1062 Ma was used as a concentration standard. The 1σ level was used for errors in the single analyses of U/Pb ratios and ages, whereas the 2σ level was used for errors in the calculated concordant ages and intercepts with the concordia. The Isoplot/Ex program was used to construct the concordia plots according to the method outlined in [28].

 doi:10.20944/preprints202406.0415.v1

Zircon trace element measurements were performed using a Cameca IMS-4f ion microprobe at the Yaroslavl' branch of the Institute of Physics and Technology of Russian Academy of Sciences. We mainly followed the analytical procedure described in [29,30]. The primary O_2^- ion beam spot size was around 20 μm. Each analysis was averaged from three measurement cycles. The precision of the trace element measurements was up to 10% for concentrations exceeding 1 ppm and up to 20% for concentrations between 0.1 and 1 ppm. To construct REE distribution spectra, the zircon compositions were normalized to that of CI chondrite [31]. The Ce and Eu anomalies were calculated using the following formulas:

$$Eu/Eu* = Eu_N/\sqrt{[(Sm_N) * (Gd_N)]} \quad (1)$$

$$Ce/Ce* = Ce_N/\sqrt{[(La_N) * (Pr_N)]}. \quad (2)$$

The zircon crystallization temperature was determined using a Ti-in-Zrn thermometer [32].

4. Results

4.1. Zircon Characterization

A total of 120 zircon grains were separated from sample 2218. Most of these grains were prismatic, although bipyramidal forms were occasionally observed. The aspect (i.e. length to width) ratio of the grains ranged from two to three (Figure 4a). The grain diameter typically ranged from 30 to 100 μm, with some grains reaching up to 150 μm. In the CL images, the central parts of the grains show dark grey coloring and pronounced oscillation zoning typical of magmatic zircon. These can be readily distinguished from the light grey inhomogeneous rims with thicknesses ranging from a few microns to 50 μm (Figure 4a). The rims are characterized by the development of cracks perpendicular to the grain boundaries, which are visible on BSE images (Figure 4b). Zircons also contain a significant number of inclusions in the zircons' cores and rims both, both primary and secondary, associated with the fracturing. The mineral inclusions are predominantly quartz, potassium feldspar, and less commonly apatite, muscovite, and epidote. In one case, a clinopyroxene inclusion with a jadeite end member content of 19% was found in the grain rim (Figure 4b). The uniformity of the zircon grains' morphology and the presence of a significant number of mineral inclusions of the zircon host rock (i.e., quartz, potassium feldspar, muscovite, and apatite) support the interpretation that the studied rocks are indeed orthogneisses and not metasediments.

 doi:10.20944/preprints202406.0415.v1

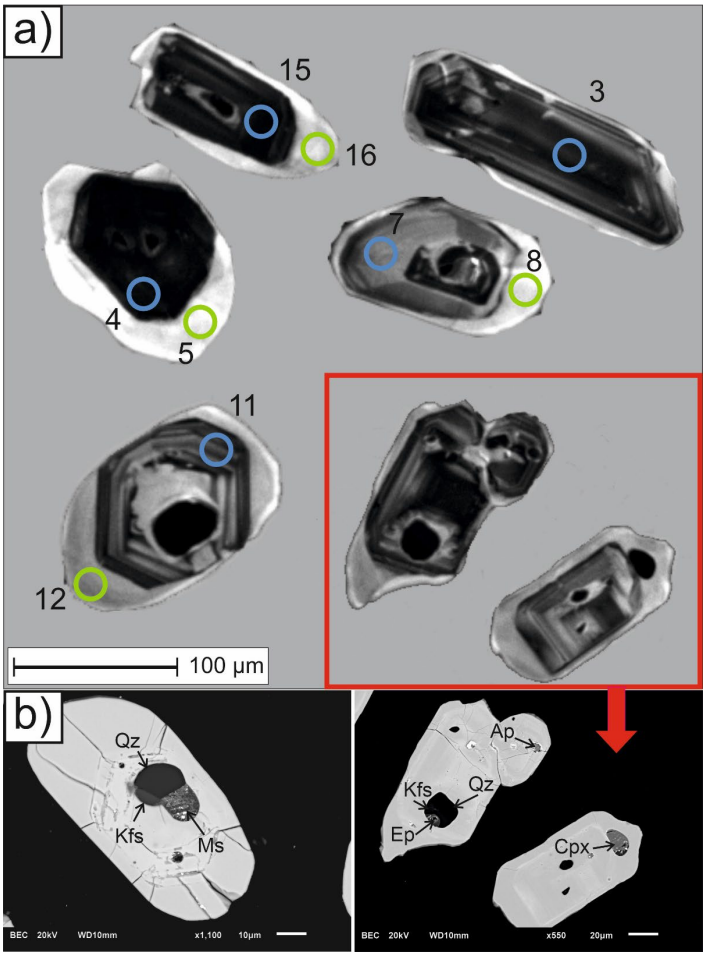

Figure 4. (a) CL images of zircons from granitic gneiss (sample 2218). Colored circles indicate the SIMS analytical spots, the numbers of which correspond to those in Table S1 and Figure 6. Blue circles indicate magmatic cores, green circles – metamorphic rims. **(b)** BSE images of zircons from granitic gneiss (sample 2218) with labeled mineral inclusions.

More than 50 zircon grains were separated from sample 2209. These grains are highly heterogeneous in both size and shape and many are fragments of crystals. The grain diameter is typically between 200 and 400 µm, and the whole grains have aspect ratios of 3–4.

In the CL images, four distinct zircon domains can be identified based on their color and internal structure (Figure 5a). The first domain is represented by zircon cores with pronounced, fine-banded oscillatory zoning, characteristic of igneous zircons. The second domain (two measurements; points 7 and 19 in Figure 5a) includes gray cores with very weakly expressed or practically absent oscillatory zoning. In the BSE images, these two domains are characterized by numerous irregularly distributed cracks, as well as mineral inclusions comprising mainly phlogopite, muscovite, amphibole, and less commonly garnet, rutile, chlorite, quartz, and potassium feldspar (Figure 5b, c). The third domain is composed of dark, monotonous zones, which may comprise almost the entire grain. In one case these zones form thick borders (up to 150 µm thick) with embayed boundaries around the core of the first domain, indicating that the grain has undergone partial melting. The fourth domain is characterized by light grey monochromatic rims of variable thickness (up to 200 µm) and veinlets, which are present in almost all the grains (Figure 5a). In the BSE images, the third and fourth domains are distinguished by the absence of cracks and inclusions (Figure 5c).

Preprints.org (www.preprints.org) | NOT PEER-REVIEWED | Posted: 7 June 2024 doi:10.20944/preprints202406.0415.v1

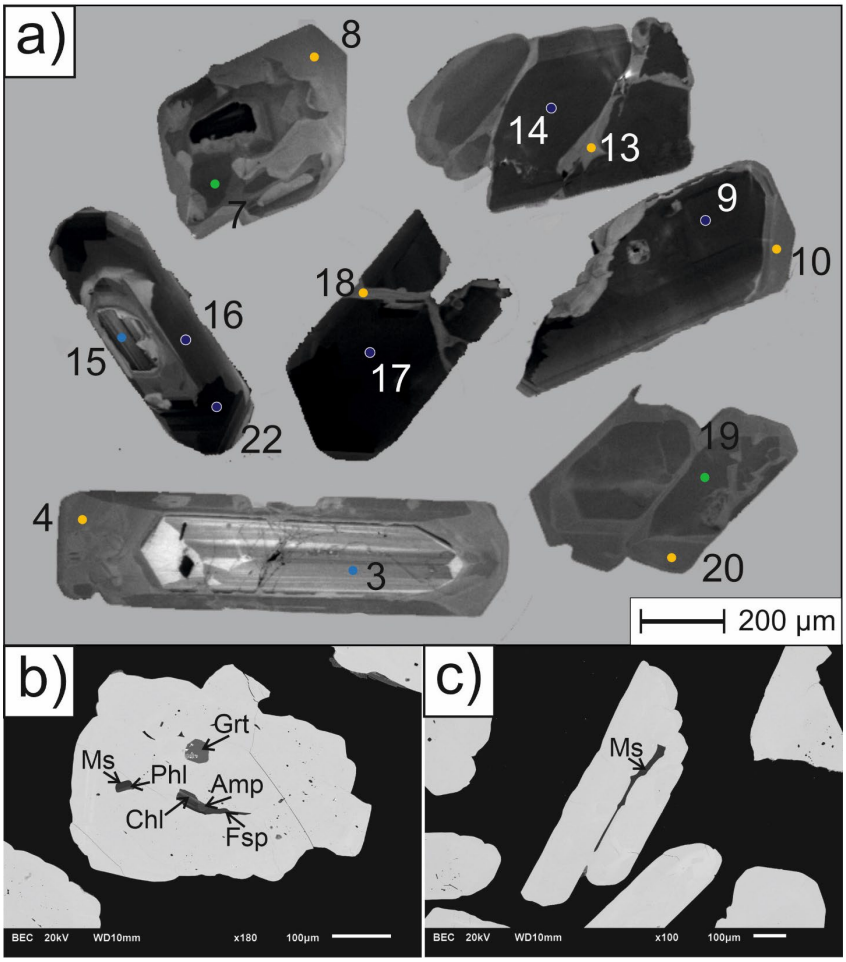

Figure 5. (a) CL images of zircons from the selvage of a pegmatite vein (sample 2209). The colored circles indicate the SIMS analytical spots, the numbers of which correspond to those in Table S2 and Figure 7. Blue circles indicate magmatic cores (1-st domain), green circles indicate recrystallized cores (2-nd domain), navy blue circles indicate pegmatite zircon (3-rd domain), yellow circles – eclogite rims and veinlets (4-th domain). **(b)** and **(c)** BSE images of zircons from the selvage of a pegmatite vein (sample 2209) with labeled mineral inclusions.

4.2. Zircon Trace Element Composition

4.2.1. Zircon from Granitic Gneisses (Sample 2218)

The cores of the zircon grains from granitic gneisses are characterized by a strongly fractionated REE distribution with a regular increase observed from light to heavy REE (Lu_N/La_N ratios from 33.1 to 11,905; Lu_N/Gd_N ratios from 10.0 to 22.1) (Figure 6a). The total REE content varies between 835 and 4210 ppm. A pronounced positive Ce anomaly (average Ce/Ce* of 20.3) and negative Eu anomaly (average Eu/Eu* of 0.18) are observed. The presence of a paired positive Ce anomaly and a negative Eu anomaly is often observed in zircons of magmatic origin. Positive Ce anomalies are associated with high oxygen fugacity in the system, while negative Eu anomalies are associated with simultaneous crystallization of plagioclase in the melt [33,34]. Furthermore, the cores of zircon grains from granitic gneisses are characterized by increased contents of certain elements, including P (272–1014 ppm), Y (1168–9591 ppm), and Li (0.24–13.4 ppm). The elevated concentrations of these elements (Figure 6a) and the strongly fractionated distribution of HREE also indicate a magmatic origin for these zircons [35]. The observed Li content >0.1 ppm and elevated P content may suggest that the zircon cores crystallized in granitoids [36,37]. Based on the Ti-in-zircon thermometer [32], the average calculated formation temperature for the zircon cores was approximately 770°C, which is broadly consistent with the temperature of granite formation [38].

Preprints.org (www.preprints.org) | NOT PEER-REVIEWED | Posted: 7 June 2024 doi:10.20944/preprints202406.0415.v1

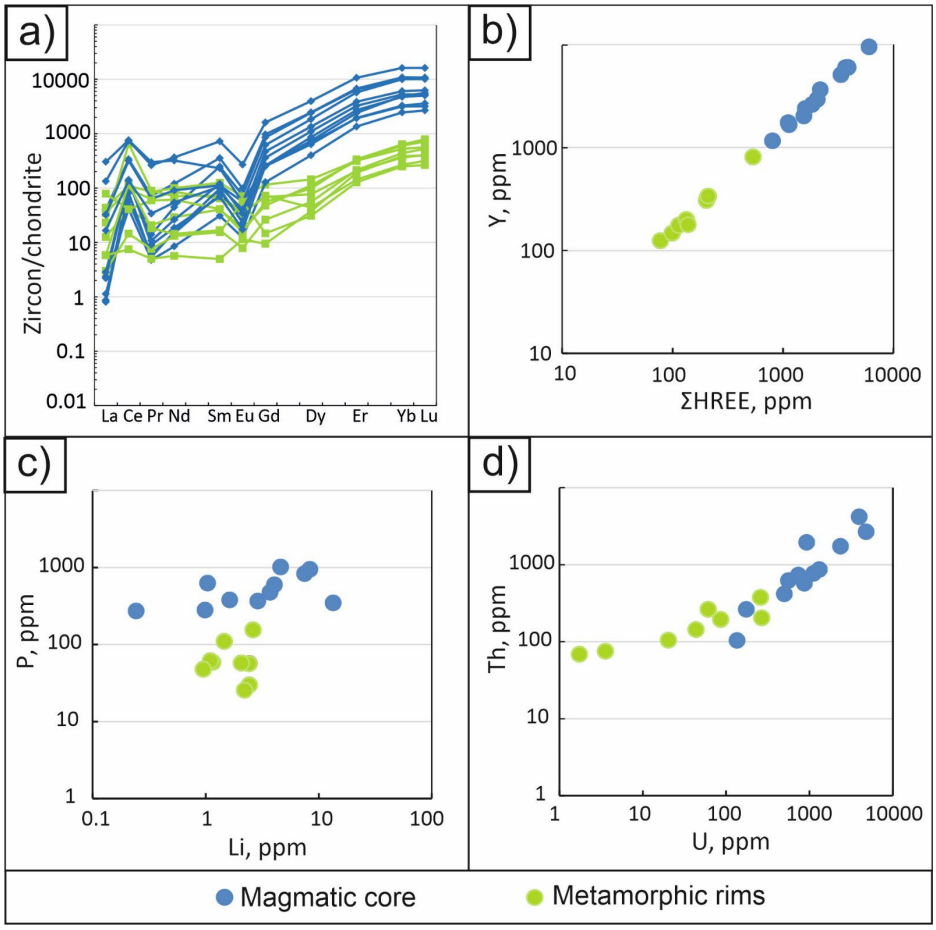

Figure 6. Trace element compositions of zircons from granitic gneiss (sample 2218). **(a)** REE distribution patterns normalized to CI chondrite [31]. **(b-d)** Co-variation diagrams of element pairs.

The REE distribution patterns of the rims of the zircon grains from granitic gneisses (Figure 6) are also differentiated; however, the spectra are flatter relative to those from the grain cores in the range from Gd to Lu (Lu_N/La_N ratio varies from 9.1 to 130, while the Lu_N/Gd_N ratio ranges from 4.38 to 42.1). The total REE content in the rims is lower than that in the cores and varies in the range of 99.0–644 ppm. The Ce anomaly remains positive in the grain rims, but its values are lower (Ce/Ce* average of 3.9). In most cases, the Eu anomaly remains negative and decreases in magnitude, with values in the range of 0.14 to 0.58 (with an average of 0.38). However, in two instances, the sign of the Eu anomaly changes to positive, with corresponding Eu/Eu* values of 1.66 and 3.71. A decrease in the value of Ce anomaly and an increase in the value of Eu anomaly relative to the zircons' cores may indicate recrystallization of zircon in the presence of fluid [33,35]. The rims of the grains also exhibit lower contents of elements such as P (25.5–155 ppm), Y (124–814 ppm), and Li (0.9–2.6 ppm). The flattening of REE spectra in the range from Gd to Lu is also characteristic of metamorphic zircon [35,39]. A decrease in the content of Y and P (Figure 6b, c) in the rims of the grains may be associated with the redistribution of these elements into accessory minerals such as allanite and apatite. The temperature value for the rims was calculated using the Ti-in-zircon thermometer approach [32], which yielded an average of approximately 740°C.

Based on these findings, we interpret that the cores of the zircon grains from granitic gneisses reflect the igneous stage of their formation, while the compositions of their rims reflect the metamorphic stage.

4.2.2. Zircon from the Selvage of a Pegmatite Vein (Sample 2209)

 doi:10.20944/preprints202406.0415.v1

The first domain within the zircon grains (i.e., zircon cores with pronounced oscillatory zoning) is characterized by differentiated REE spectra, with an increase in the content from light to heavy REE. The Lu_N/La_N ratio varies from 3955 to 15,027, while the Lu_N/Gd_N ratio varies from 10.4 to 18.3 (Figure 7a). The total REE content is lower than in the zircon cores from granitic gneisses, with values ranging from 467 to 1342 ppm. A prominent positive Ce anomaly (Ce/Ce* average of 53.3) and negative Eu anomaly (Eu/Eu* average of 0.22) are observed. As discussed above, in the cores of zircon grains from granitic gneisses, the differentiated REE spectra, positive Ce anomalies, and negative Eu anomalies likely indicate the magmatic genesis of these zircons. The contents of Y (655–2117 ppm), P (185–338 ppm), and Li (0.02–0.42 ppm) are lower than those recorded in the zircon cores from granitic gneisses (Figure 7b,c). The lower contents of HFSE and P relative to zircon cores from granitic gneisses, in addition to the Li content of <0.1 ppm in all grains except one, may indicate that the first domain cores were crystallized in basic rocks of the oceanic crust [36,37]. Geochemical discriminant diagrams [40] indicate that these zircons fall within the region of overlap between the oceanic and continental crust (Figure 8). It is assumed that the zircons from the first domain belong to the igneous protolith of the eclogites and were captured by the pegmatite melt.

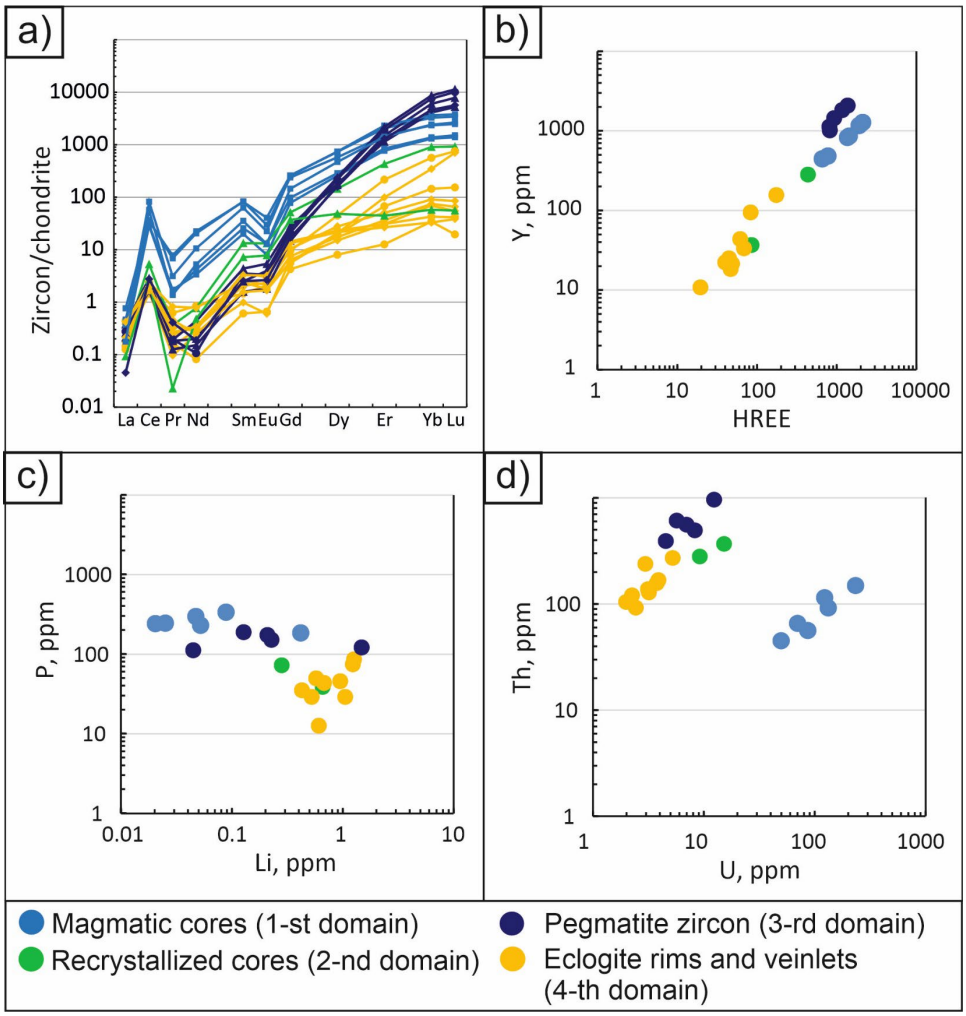

Figure 7. Trace element compositions of zircons from the selvage of a pegmatite vein (sample 2209). **(a)** REE distribution patterns normalized to CI chondrite [31]. **(b-d)** Co-variation diagrams of element pairs.

Preprints.org (www.preprints.org) | NOT PEER-REVIEWED | Posted: 7 June 2024 doi:10.20944/preprints202406.0415.v1

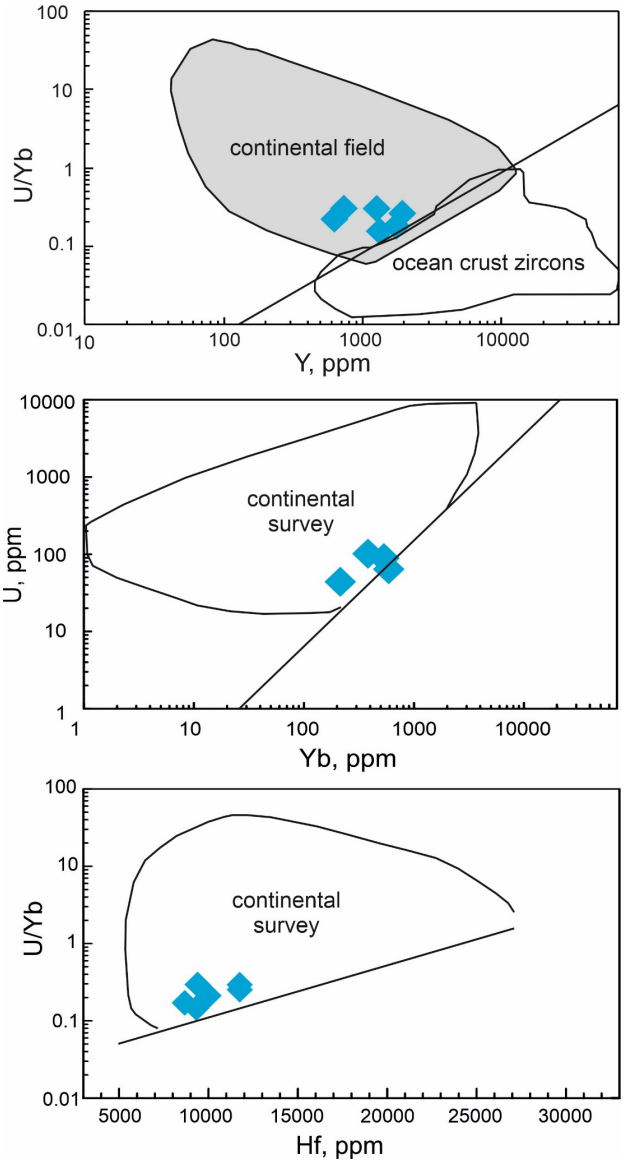

Figure 8. Geochemical discriminant diagrams for zircon after [40]. Blue markers indicate the positions of zircon cores from the selvage of the pegmatite vein (sample 2209).

Figure 7a in the case of zircon from the second domain, a positive Ce anomaly (Ce/Ce* of 19.0 and 57.3) and a negative Eu anomaly (Eu/Eu* of 0.48 and 0.50) are observed. The total REE content values are lower than that recorded in the cores of the first domain, with values of 40.2 and 288 ppm. Furthermore, this zircon domain is distinguished by an increase in the Li content (0.28 and 0.66 ppm) and a decrease in the Y content (85.4 and 336 ppm) and P content (39.0 and 73.0 ppm) relative to the first domain (Figure 7b,c). We suggest that the second zircon domain corresponds to the recrystallization of zircons from the first domain, with the preservation of some of their geochemical characteristics.

The third zircon domain (i.e., dark, unzoned zircons when viewed in CL) is distinguished by the most sharply differentiated REE spectra of all four domains, with Lu_N/La_N ratios ranging from 13,926 to 125,367 and Lu_N/Gd_N ratios ranging from 185 to 532 (Figure 7a). The total REE content is also high, ranging from 1019 to 2082 ppm. Furthermore, the REE spectra exhibit a prominent positive Ce anomaly (average Ce/Ce* of 12.3) and a weakly negative Eu anomaly (average Eu/Eu* of 0.43). The content of Y varies between 806 and 1374 ppm, P between 112 and 189 ppm, and Li between 0.04 and 1.47 ppm (with an average of 0.42 ppm). The overall character of the REE distribution, along with the high observed Y and P values (Figure 7b, c), indicates that this zircon domain was formed during crystallization of the pegmatite [41–43], i.e., this zircon is true pegmatitic zircon. The temperature

 doi:10.20944/preprints202406.0415.v1

value for this domain was calculated using the Ti-in-zircon thermometer [Watson et al., 2006], which yielded an average of approximately 700 °C. This value is broadly consistent with the typical formation temperature of pegmatites [44].

The fourth zircon domain, which forms the late rims and veinlets, is characterized by weakly differentiated REE spectra. In most cases, the slope of the HREE distribution is less steep than samples from the other domains, with the Lu_N/La_N ratio varying from 108 to 5182 and the Lu_N/Gd_N ratio varying from 2.90 to 119. The total REE content is lower than in all the other domains, with values ranging from 11.9 to 158 ppm. The REE spectra are characterized by the presence of a positive Ce anomaly (average Ce/Ce* of 7.96) and a weak negative Eu anomaly (average Eu/Eu* of 0.46). The values of the Ce and Eu anomalies are lower than those in the magmatic zircons of the first domain (Figure 7a). A decrease in the total REE content, particularly HREE, as well as a decrease in the magnitudes of the Ce and Eu anomalies, suggests that zircon from this domain formed during the recrystallization of magmatic zircon under eclogite facies metamorphism [35,39]. Zircon from this domain exhibits a lower P (12.7–86.7 ppm) and Y (19.5–174 ppm) content relative to the magmatic cores of the first domain (Figure 7b, c), whereas the Li content in the fourth domain is higher (Li = 0.426–1.26 ppm). The reduced Y and P contents are also indicative of eclogitic zircon [35].

4.3. Zircon U-Pb Geochronology

4.3.1. Zircon from Granitic Gneisses (Sample 2218)

A concordant age value of 471 ± 2 Ma was determined for magmatic cores in zircon from granitic clay based on 13 points (MSWD = 1, Figure 9). The U content varies between 71.3 and 3538 ppm, while the Th content ranges from 94.7 to 5120 ppm. The Th/U ratio varies within the range of 0.64–2.49, i.e., >0.1 in all cases, which indirectly indicates the magmatic genesis of this zircon [45].

A concordant age was established from the metamorphic zircon rims at seven points, with an age of 370 ± 4 Ma (MSWD = 0.16, Figure 9). The U and Th contents were lower in the rims relative to the cores, with values of 51.6–105 ppm and 0.48–6.90 ppm, respectively. The Th/U ratio falls within the range of 0.01–0.10, which provides further evidence for the metamorphic genesis of this zircon [46].

Preprints.org (www.preprints.org) | NOT PEER-REVIEWED | Posted: 7 June 2024 doi:10.20944/preprints202406.0415.v1

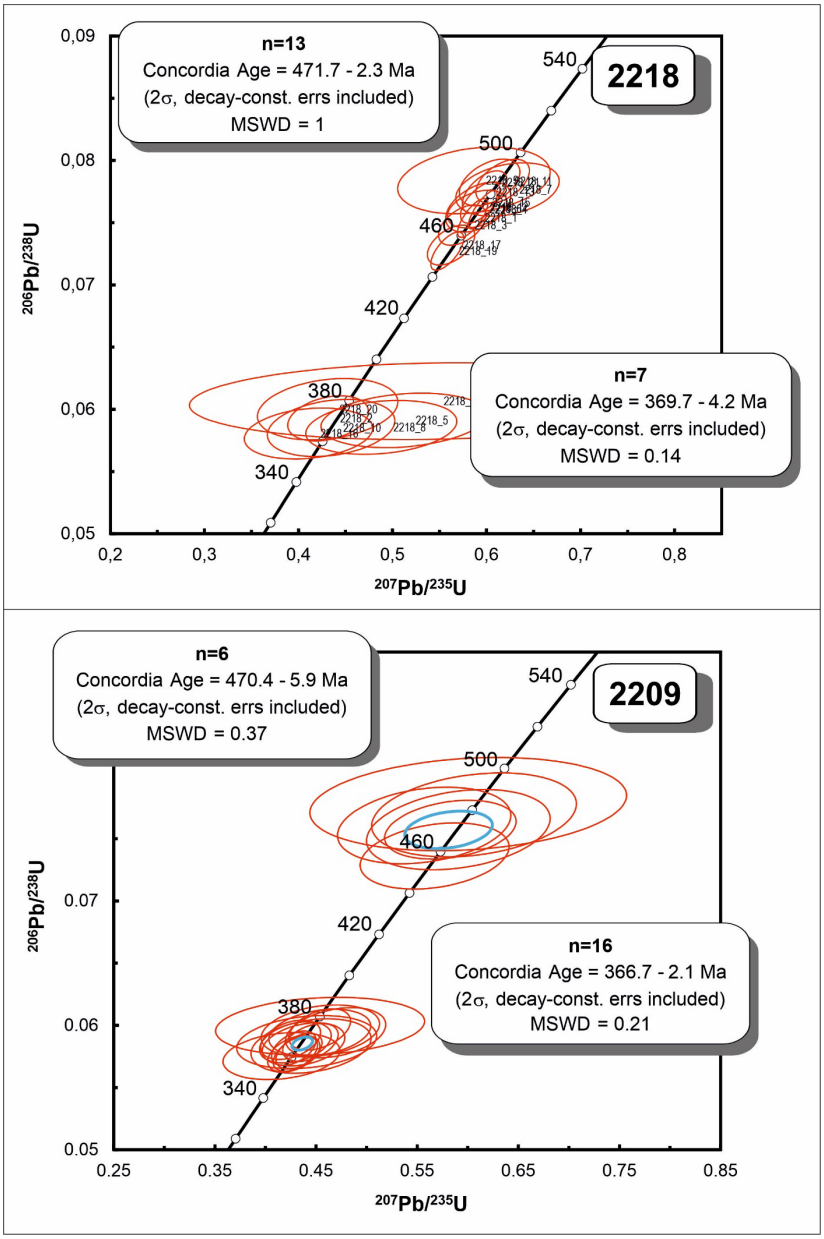

Figure 9. Concordia plot for zircons **(a)** from granitic gneiss (sample 2218) and **(b)** from the selvage of a pegmatite vein (sample 2209).

4.3.2. Zircon from the Selvage of a Pegmatite Vein (Sample 2209)

For the first domain of the zircons from the pegmatite vein selvage, a concordant age of 470 ± 6 Ma was determined based on six points (MSWD = 0.36, Figure 9a). The U and Th contents are lower than those recorded in the magmatic zircon cores from granitic gneisses (U = 31.7–94.8 ppm; Th = 48.1–187 ppm). The Th/U ratio varies within the range of 0.90–2.29, with all values exceeding 0.1, which may imply the magmatic genesis of these zircons [45].

The remaining three zircon domains, collectively comprising 16 points, yield a concordant age of 367 ± 2 Ma (MSWD = 0.21, Figure 9b). There is a considerable disparity in the U and Th contents observed across the different zircon domains. Zircons of the second domain, interpreted as recrystallized igneous cores, exhibit an elevated U content (170 and 254 ppm) and a reduced Th content (7.16 and 13.8 ppm) compared to the igneous cores of the first domain. Zircon of the third domain, characteristic of pegmatitic zircon, displays the highest U content (73.6–542 ppm), while, the Th content varies within the range of 2.07–7.98 ppm. Zircon of the fourth domain (eclogitic zircon) is characterized by a lower Th content relative to the magmatic cores of the first domain (1.63–6.17

 doi:10.20944/preprints202406.0415.v1

ppm), while the U content is higher (U = 60.7–281 ppm). The Th/U ratio is notably low in this domain (0.02–0.03), which is typical of metamorphic zircon [46].

5. Discussion

5.1. Metamorphic Rims of Zircon from Granitic Gneiss: A Result of Eclogite Metamorphism?

Given the concurrence in age between the metamorphic rims of the zircon samples derived from granitic gneisses and those from the eclogite rims within zircon samples from pegmatite veins, it is important to consider whether eclogite metamorphism has been superimposed upon granitic gneisses or whether the Marun-Keu complex represents a later amalgamation of metamorphic rocks subjected to varying conditions.

Metagranitoids and quartzo-feldspathic gneisses frequently serve as the host rocks for eclogites within various high-pressure (HP) and ultrahigh-pressure (UHP) complexes, as evidenced in studies from regions such as the Western Gneiss Region [47], the Belomorian Mobile Belt [48], the Muya block eclogites [49], and the Tso Morari massif [50]. The Marun-Keu is also an example of this type of complex [3]; however, a significant challenge remains in determining the pressure–temperature (P-T) conditions of these supposedly HP acidic rocks, which raises questions about their involvement in HP and UHP metamorphic processes. Researchers frequently focus on eclogites that originate from mafic and ultramafic rocks because the formation of eclogite parageneses and eclogite index minerals is typically hindered in granitoids due to their composition and fluid imbalance [47,50,51]. Furthermore, in certain instances, eclogite parageneses may be obliterated during subsequent retrograde metamorphism associated with rock dehydration, which occurs in metagranitoids [52].

The identification of isolated small garnet grains within the granitic gneisses, as well as the observation of Na-pyroxene inclusions in the metamorphic rim of their zircons (with a jadeite mineral content of 19%), suggests that the metamorphic evolution of the studied granitic gneiss may have occurred under eclogite facies conditions, albeit at a relatively modest P-T configuration. This scenario suggests that omphacite may have crystallized within the granitic gneiss during eclogite metamorphism; however, subsequent retrograde metamorphism has likely led to its dissolution or alteration, resulting in the absence of omphacite in the rock's current mineral assemblage.

The observed flattening of the REE spectra in the HREE range in the rims of zircons from granitic gneisses compared to their magmatic cores, and the variations in trace element composition, including decreases in Th, P, Y, and Li content in the rims, are consistent with the known behavior of these elements during zircon recrystallization in response to eclogite metamorphism in basic rocks [35,39]. Based on these observations, we interpret that the metamorphic rims of the zircons from the granitic gneisses were formed during the recrystallization of igneous zircon during eclogite metamorphism. We also interpret that the rock itself was involved in eclogite metamorphism, along with the mafic and ultramafic rocks common in this area.

5.2. Discussion of Geochronological Data

As previously stated, the dating of eclogites and related rocks from the Marun-Keu area has been conducted by various authors [3,10,12–15]. The data obtained by all the listed authors are summarized in Table 1.

Table 1. Summary of published rock age estimates from the Marun-Keu complex.

Type of rock	Dating method	Age	Authors, year
Age of metamorphism			
Granitic gneisses	K-Ar	250 – 417 Ma	Udovkina, 1971, 1985
Eclogites	Sm-Nd	338 – 366 Ma	Shatskii et al., 2000
Kyanite eclogites	U-Pb	351 – 385Ma	Meng et al., 2020
Eclogites	Rb-Sr and Sm-Nd	1.54 – 1.69 Ga	Andreichev et al., 2007

 doi:10.20944/preprints202406.0415.v1

Eclogites, metagranitoids, garnet amphibolites etc.	Rb-Sr	352 – 360 Ma	Glodny et al., 2003
Metagranites, metamorphic rim in eclogite facies vein	U-Pb	353 – 375 Ma	Glodny et al., 2004
Eclogites (after gabbro and peridotites); garnet peridotites forming	K-Ar	439 – 650 Ma	Udovkina, 1971, 1985
Rutile eclogite	U-Pb	750 – 1700 Ma	Udovkina, 1985
Eclogite protoliths			
Olivine gabbro, gabbro-norites, peridotites	K-Ar	600 – 800 Ma	Udovkina, 1971, 1985
Gabbro, troctolites	U-Pb	420 – 508 Ma	Meng et al., 2020
Gabbro	Rb-Sr	467 Ma	Glodny et al., 2003
Dolerites/Gabbro (?)	U-Pb	481 – 542 Ma	Glodny et al., 2004
Metagranitoids protoliths (granitic gneisses)			
Granitoids	U-Pb	470 – 670 Ma	Glodny et al., 2004
Granitoids	U-Pb	481 – 527 Ma	Udoratina et al., 2021
Granitoids	K-Ar, U-Pb	525 – 780 Ma	Udovkina, 1971, 1985
Pegmatites cutting eclogite bodies			
Pegmatites and quarz-muscovite veins	K-Ar	271 – 500 Ma	Udovkina, 1971, 1985
Quarz-plagioclase-muscovite veins (?)	Rb-Sr	356 – 358 Ma	Glodny et al., 2003

5.2.1. Age of the Eclogite Protolith

Using the K-Ar method for olivine gabbros, gabbro-norites, and peridotites, Udovkina [3,11] obtained age values ranging from 800 to 600 Ma (Table 1) for the protoliths of eclogites. Additionally, the Rb-Sr dating method applied to relict gabbro samples yielded an age of approximately 467 Ma [13]. An analysis of magmatic zircon cores within kyanite eclogites using the U-Pb system revealed ages spanning 508–420 Ma, which were interpreted by the authors as representing the time of formation of the original gabbro/troctolite [15]. In addition, individual igneous zircon grains extracted from a mafic eclogite specimen exhibited ages falling within the range of 542–481 Ma [14].

In the present study, the age of the magmatic zircon cores retrieved from the selvage of a pegmatite vein (470 Ma) is interpreted as representative of the eclogite protolith's age. This finding is consistent with previous dating results reported by Glodny et al. [13] and Meng et al. [15]. The observed variability in the ages attributed to the eclogite protoliths may relate to the tectonic juxtaposition of protoliths originating from distinct temporal periods.

5.2.2. Age of the Host Rock Protolith (Granitic Magmatism)

Using the U-Pb system, age values of 470–670 Ma were obtained for a heterogeneous population of igneous zircons from metagranitoids [14]. The authors linked a cluster of zircon grains with an age of ~490 Ma to the tectonic rifting phase associated with the development of the Paleo-Ural Ocean and the Early Paleozoic East European passive margin. It was assumed that the source of these granitoids could be island-arc type crust [14].

In the Urals region, Udoratina et al. [53] delineated two significant categories of granitoids: the pre-Uralids, which were formed prior to the fold belt's formation with ages ranging from 735 to 480 Ma, and the Uralids, characterized by ages ranging from 460 to 249 Ma. The formation of A-type granitoids within the Marun-Keu complex is attributed to rift-related magmatism of 520–480 Ma age, which coincides with the age of the pre-Uralid granitoids, a conclusion that is consistent with the findings of Glodny et al. [14].

The age obtained in this work for magmatic zircon cores from granitic gneisses (470 Ma) may be ascribed to the transitional period marking a shift in tectonic conditions from a rift-related setting to an island-arc environment.

5.2.3. Age of Eclogite Metamorphism

 doi:10.20944/preprints202406.0415.v1

The studies by Udovkina in 1971 and 1985 provide insights into the age determination of eclogites through the application of the K-Ar method, yielding ages ranging from 650 to 439 Ma. In a subsequent study [10], the Rb-Sr and Sm-Nd methods were employed to determine the age of eclogites, resulting in an age range of 1.69–1.54 Ga. This suggests that this timeframe is the probable period of "primary crystallization of eclogites" [10]. Ancient dating was also obtained using the U-Pb method on zircons from a sample of rutile eclogite (1700–750 Ma) [11]. Highly consistent age estimates of eclogites were also obtained from the Sm-Nd method (366–338 Ma) [12], the U-Pb method (385–351 Ma) [14,15], and the Rb-Sr method (360–352 Ma) [13]. The age of metamorphic zircon is interpreted as the time of arc-continental collision due to the eastward subduction of the East European passive margin [14].

The age determination of host rocks using the K-Ar method yielded dates with marked variability ranging from 417 to 250 Ma [3,11]. This variation in age estimates likely relates to the complex nature of multiphase granitization and migmatization processes affecting the host rocks, as highlighted by Udovkina and the authors of the present study. These processes can potentially lead to disturbances in the K-Ar isotopic system. The metamorphic ages of the metagranitoids, as determined using the Rb-Sr and U-Pb systems, demonstrate close agreement within the range of 375–353 Ma [13,14].

In the present study, we obtained an eclogitization age close to those described above (about 370 Ma); thus, it is assumed that eclogite metamorphism was reflected not only in the tectonic blocks composed of basic and ultrabasic rocks but also in the acidic host rocks.

5.2.4. Age of Pegmatites

The ages of the pegmatites and quartz–muscovite veins that cut the eclogite bodies were estimated using the K-Ar method, yielding age values ranging from 500 to 271 Ma [3,11]. In a more recent study, Glodny et al. [13] used the Rb-Sr method to analyze samples from veins comprising primarily quartz, muscovite, and feldspars, resulting in estimated ages of 358–356 Ma.

Based on field observations, the pegmatites are the youngest formations in the study area; however, our date estimates (about 370 Ma), in turn, indicate that the processes of eclogitization and the intrusion of pegmatite veins were approximately simultaneous, which is also confirmed by the data obtained in [13]. The question regarding the source material for the formation of the pegmatites remains open. The near-simultaneous eclogite metamorphism and crystallization of pegmatites do not exclude partial melting of some areas of the host granitoids during metamorphism. The pegmatitic zircon described in this work, with the exception of one grain, does show no evidence of magmatic cores that would indicate granitoid magmatism with an age of 470 Ma. The only grain identified in this study with a magmatic core of 470 Ma age may have been captured from the host acid rocks rather than a relic left from the melting of the rocks. Consequently, the question of the source of the material for the pegmatites remains unresolved and requires further investigation.

6. Conclusion

In this study, zircons from the Marun-Keu complex are investigated to determine the timing and nature of igneous and metamorphic processes in the study area. The zircons separated from the granitic gneisses exhibited magmatic cores with an age of 470 Ma, in addition to metamorphic rims with an age of around 370 Ma. The magmatic cores exhibit typical geochemical features of zircons from acid rocks, such as increased content of P (272–1014 ppm), Y (1168–9591 ppm), Li (0.24–13.4 ppm), and Th (94.7–5120 ppm), a strongly fractionated REE distribution, a significant positive Ce anomaly (Ce/Ce* average of 20.3) and a negative Eu anomaly (Eu/Eu* average of 0.18). In contrast, the metamorphic rims of the zircon grains from the granitic gneisses demonstrate features typical of eclogitic zircon, including decreased content of P (25.5–155 ppm), Y (124–814 ppm), Li (0.9–2.6 ppm), and Th (0.48–6.97 ppm), flattened REE patterns in the HREE region, decreased magnitude of Ce anomalies, and increased magnitude of Eu anomalies relative to the magmatic core. Additionally, we identified four distinct domains of heterogeneous zircon separated from the selvage of the pegmatite vein: 1) magmatic cores of approximately 470 Ma age exhibiting geochemical features typical of

 doi:10.20944/preprints202406.0415.v1

zircons crystallized in basic rocks, such as reduced P (185–338 ppm), Y (655–2117 ppm), Li (0.02–0.42 ppm), and Th (48.1–187 ppm) content relative to zircon cores from granitic gneisses, differentiated REE pattern, positive Ce anomaly and negative Eu anomaly; 2) zircons that recrystallized during eclogite metamorphism, exhibiting geochemical characteristics intermediate between those of the magmatic cores and true eclogitic zircon; 3) pegmatitic zircon with the most strongly fractionated REE distribution among the four domains, featuring a pronounced positive Ce anomaly (average Ce/Ce* of 12.3) and a weakly negative Eu anomaly (average Eu/Eu* of 0.43), Y content of 806–1374 ppm, P content of 112–189 ppm, an average Li content of 0.42 ppm, and Th content of 2.07–7.98 ppm; and 4) eclogitic zircon in the form of veinlets and rims that overlay the three aforementioned domains, characterized by low P (12.7–86.7 ppm), Y (19.5–174 ppm), and Th (1.63–6.17 ppm) content, weakly fractionated distributions of REE with HREE depletion, and decreased magnitudes of Ce and Eu anomalies relative to the magmatic cores. The ages of the last three domains coincide within the error limits, indicating that the eclogite metamorphism and pegmatite formation processes that occurred at around 370 Ma were synchronous.

Supplementary Materials: The following supporting information can be downloaded at the website of this paper posted on Preprints.org. Table S1: Trace elements composition of representative zircon from granitic gneiss (sample 2218) by SIMS (in ppm); Table S2: Trace elements composition of representative zircon from selvage of pegmatite vein (sample 2209) by SIMS (in ppm); Table S3: Zircon U-Pb SIMS data (sample 2218); Table S4: Zircon U-Pb SIMS data (sample 2209).

Author Contributions: Conceptualization, Salimgaraeva L.I. and Berezin A.V.; methodology, Sergeev S.A.; field works, Salimgaraeva L.I., Berezin A.V., Gubanov N.V., Skublov S.G.; writing—original draft preparation, Salimgaraeva L.I.; writing—review and editing, Berezin A.V., Gubanov N.V., Skublov S.G., Steckaya E.V.; visualization, Steckaya E.V.; supervision, Skublov S.G.; funding acquisition, Gubanov N.V. All authors have read and agreed to the published version of the manuscript.

Funding: This research was funded by Russian Science Foundation, grant number 22-17-00177. Sample preparation was supported by a state assignment of the IGG UB RAS (124020400013-1).

Acknowledgments: We thank Olga Galankina for assistance with the BSE images of zircons, Evgeny Potapov and Sergey Simakin assisted with measuring of zircon trace element compositions. Two anonymous reviewers provided valuable comments that improved the quality of the report.

Conflicts of Interest: The authors declare no conflicts of interest.

References

1. Ivanov, K.S.; Puchkov, V.N. Structural-Formational Zoning of the Ural Fold Belt: An Overview and New Approach. *Geotectonics*. **2022**, *56*, 747–780. https://doi.org/10.1134/S0016852122060036.
2. Dobretsov, N.L.; Sobolev, N.V. Eclogites from metamorphic complexes of the USSR. *Physics of the Earth and Planetary Interiors*. **1970**, *3*, 462–470. https://doi.org/10.1016/0031-9201(70)90089-0.
3. Udovkina, N.G. Eclogites of the Polar Urals (on the example of the southern part of the Marun-Keu region);Moscow: Nauka,1971, 191 p.
4. Molina, J.F.; Austrheim, H.; Glodny, J.; Rusin, A. The eclogites of the Marun–Keu complex, Polar Urals (Russia): Fluid control on reaction kinetics and metasomatism during high P metamorphism. *Lithos*. **2002,** *61*, 55-78. https://doi.org/10.1016/S0024-4937(02)00070-1.
5. Molina, J.F.; Poli, S.; Austrheim, H.; Glodny, J.; Rusin, A. Eclogite-facies vein systems in the Marun-Keu complex (Polar Urals, Russia): Textural, chemical and thermal constraints for patterns of fluid flow in the lower crust. *Contributions to Mineralogy and Petrology*. **2004**, *147*, 484–504. https://doi.org/10.1007/s00410-004-0569-z.
6. Shmelev, V.R.; Meng, F.C. Evidence of Ultrahigh-Pressure Evolution of Garnet Peridotites in the Polar Urals. *Dokl. Earth Sciences*.**2023**, *513*, 1167–1172. https://doi.org/10.1134/S1028334X2360175X.
7. Selyatitskii, A.Y.; Kulikova, K.V. The first evidence of UHP metamorphism in the Polar Urals (Russia). *Dokl. Earth Sciences.* **2017**, *476*, 1222–1225. https://doi.org/10.1134/S1028334X17100270.
8. Liu, Y.Y.; Perchuk, A.L.; Ariskin, A.A. High pressure metamorphism in the peridotitic cumulate of the Marun-Keu Complex, Polar Urals. *Petrology* **2019**, *27*, 124-145. https://doi.org/10.1134/S0869591119020061.
9. Liu, Y.Y.; Perchuk, A.L.; Philippot, P. Eclogites from the Marun-Keu Complex, Polar Urals, Russia: A record of hot subduction and sub-isothermal exhumation. *Geological Society, London, Special Publications*. **2019,** *474,* 255-274. https://doi.org/10.1144/SP474.6.

10. Andreichev, V.L.; Ronkin, Y.L.; Serov, P.A.; Lepikhina, O.P.; Litvinenko, A.F. New data on the Precambrian age of Marunkeu eclogites (Polar Urals). *In Doklady Earth Sciences,Springer Nature BV*. **2007**, *413*, 347. *https://doi.org*/10.1134/S1028334X07030051.
11. Udovkina, N.G. *Eclogites of the USSR;*Moscow: Nauka, 1985, 288 p.
12. Shatskii, V.S.; Simonov, V.A.; Jagoutz, E.; Kurenkov, S. A.; Koz'menko, O. A. New data on the age of eclogites from the Polar Urals. *In Doklady Earth Sciences*. **2000**, *371*, 534–538.
13. Glodny J.; Austrheim H.; Molina J.F.; Rusin A.I.; Seward D. Rb/Sr record of fluid-rock interaction in eclogites: The Marun-Keu complex, Polar Urals, Russia. *Geochimica et Cosmochimica Acta*. **2003**, *67*, 4353–4371. https://doi.org/10.1016/S0016-7037(03)00370-3.
14. Glodny J.; Pease V.; Montero P.; Austrheim H.; Rusin A.I. Protolith ages of eclogites, Marun-Keu Complex, Polar Urals, Russia: Implications for the pre- and early Uralian evolution of the northeastern European continental margin. *Geol. Soc. Lond. Memoirs.* **2004**, *30*, 87–105. *https://doi.org*/10.1144/GSL.MEM.2004.030.01.
15. Meng F.; Fan Y.; Shmelev V.R.; Kulikova K.V. Constraints of eclogites from the Marun-Keu metamorphic complex on the tectonic history of the Polar Urals (Russia). *J. Asian Earth Sciences*. **2020**, *187*, 104087. https://doi.org/10.1016/j.jseaes.2019.104087.
16. Bosse, V.; Villa, I.M. Petrochronology and hygrochronology of tectono-metamorphic events. *Gondwana Research.***2019**, *71*, 76-90. https://doi.org/10.1016/j.gr.2018.12.014.
17. Chen, R.X.; Zheng, Y.F. Metamorphic zirconology of continental subduction zones. *J. Asian Earth Sci.* **2017**, *145*, 149–176. https://doi.org/10.1016/j.jseaes.2017.04.029.
18. Kohn, M.J.; Corrie, S.L.; Markley, C. The fall and rise of metamorphic zircon. *Am. Mineral.* **2015**, *100*, 897–908. https://doi.org/10.2138/am-2015-5064.
19. Skublov, S.G.; Levashova, E.V.; Mamykina, M.E.; Gusev, N.I.; Gusev, A.I. The polyphase Belokurikhinsky granite massif, Gorny Altai: Isotope-geochemical study of zircon. *J. Min. Institute.***2024,** EDN RGKCIJ.
20. Skublov, S.G.; Petrov, D.A.; Galankina, O.L.; Levashova, E.V.; Rogova, I.V. Th-Rich Zircon from a Pegmatite Vein Hosted in the Wiborg Rapakivi Granite Massif. *Geosciences* **2023**, *13*, 362. https://doi.org/10.3390/geosciences13120362.
21. Black, L.P.; Kamo, S.L.; Allen, C.M.; Davis, D.W.; Aleinikoff, J.N.; Valley, J.W.; Mundil, R.; Campbell, I.H.; Korsch, R.J.; Williams, I.S.; Foudoulis, C. Improved $^{206}Pb/^{238}U$ microprobe geochronology by the monitoring of a trace-element-related matrix effect; SHRIMP, ID-TIMS, ELA-ICP-MS and oxygen isotope documentation for a series of zircon standards. *Geosci. J.* **2004**, *13*, 245–256. https://doi.org/10.1007/s12303-009-0024-2.
22. Wiedenbeck, M.A.P.C.; Alle, P.; Corfu, F.; Griffin, W.L.; Meier, M.; Oberli, F.V.; Quadt, A.V.; Roddick, J.C.; Spiegel, W. Three natural zircon standards for U-Th-Pb, Lu-Hf, trace element and REE analyses. *Geostandards newsletter*. **1995**, *19*, 1–23. https://doi.org/10.1111/j.1751-908X.1995.tb00147.x.
23. Warr, L.N. IMA–CNMNC approved mineral symbols. *Mineral. Mag.* **2021**, *85*, 291–320. https://doi.org/10.1180/mgm.2021.43.
24. Williams, I.S.U-Th-Pb geochronology by ion microprobe. In: In: McKibben, M.A., Shanks W.C III, Ridley, W.I. (eds.). Applications of Microanalytical Techniques to Understanding Mineralizing Processes. *Rev. Econ. Geol.***1998**, *7*, 1–35. https://doi.org/10.5382/Rev.07.01.
25. Schuth, S.; Gornyy, V.I.; Berndt, J.; Shevchenko, S.S.; Karpuzov, A.F.; Mansfeldt, T. Early proterozoic U-Pb zircon ages from basement gneiss at the Solovetsky archipelago, White Sea, Russia. *Int. J. Geosci.* **2012**, *3*, 289.
26. Ludwig, K.R. Usersmanual for Isoplot/Ex rev. 2.49. *Berkeley Geochronol. Cent. Spec. Publ.* **2001**, *1*, 1–56. 439.
27. Black, L.P.; Kamo, S.L.; Allen, C.M.; Aleinikoff, J.N.; Davis, D.W.; Korsch, R.J.; Foudoulis, C. TEMORA 1: A new zircon standard for Phanerozoic U-Pb geochronology. *Chem. Geol.* **2003**, *200*, 155–170. https://doi.org/10.1016/S0009-2541(03)00165-7.
28. Ludwig, K.R. User's manual for IsoPlot 3.0. A geochronological toolkit for Microsoft Excel. **2003**, *71*, 36.
29. Dokukina, K.A.; Kaulina, T.V.; Konilov, A.N.; Mints, M.V.; Van, K.V.; Natapov, L.; Belousova, E.; Simakin, S.G.; Lepekhina E.N. Archaean to Palaeoproterozoic high-grade evolution of the Belomorianeclogite province in the Gridino area, Fennoscandian Shield: Geochronological evidence. *Gondwana Res.* **2014**, *25*, 585–613. https://doi.org/10.1016/j.gr.2013.02.014.
30. Fedotova, A.A.; Bibikova, E. V.; Simakin, S.G. Ion-microprobe zircon geochemistry as an indicator of mine ral genesis during geochronological studies. *Geochem. Int.* **2008**, *46*, 912–927. https://doi.org/10.1134/S001670290809005X.
31. McDonough, W.F.; Sun, S.-S. The composition of the Earth. *Chem. Geology.* **1995**, *120*, 223–253. https://doi.org/10.1016/0009-2541(94)00140-4.
32. Watson, E.B.; Wark, D.A.; Thomas, J.B. Crystallization thermometers for zircon and rutile. *Contrib. Mineral. Petrol.* **2006**, *151*, 413–433. https://doi.org/10.1007/s00410-006-0068-5.
33. Hoskin, P.W.; Schaltegger, U. The composition of zircon and igneous and metamorphic petrogenesis. *Rev. Mineral. Geochem.* .**2003**, *53*, 27-62. https://doi.org/10.2113/0530027.

34. Yakymchuk, C.; Holder, R.M.; Kendrick, J.; Moyen, J. F. Europium anomalies in zircon: A signal of crustal depth? *Earth Planet. Sci. Lett.* **2023**, *622*, 118405. https://doi.org/10.1016/j.epsl.2023.118405.
35. Skublov, S.G.; Berezin, A.V.; Berezhnaya, N.G. General relations in the trace-element composition of zircons from eclogites with implications for the age of eclogites in the Belomorian Mobile Belt. *Petrology*.**2012**, *20*, 427-449. https://doi.org/10.1134/S0869591112050062.
36. Belousova, E.A.; Griffin, W.L.; O'Reilly, S.Y.; Fisher, N.L. Igneous zircon: Trace element composition as an indicator of source rock type. *Contrib. Mineral. Petrol.* **2002**, *143*, 602–622. https://doi.org/10.1007/s00410-002-0364-7.
37. Ushikubo, T.; Kita, N.T.; Cavosie, A.J.; Wilde, S.A.; Rudnick, R.L.; Valley, J.W. Lithium in Jack Hills zircons: Evidence for extensive weathering of Earth's earliest crust. *Earth and Planetary Science Letters*. **2008**, *272*, 666–676. https://doi.org/10.1016/j.epsl.2008.05.032.
38. Whitney, J.A. The origin of granite: The role and source of water in the evolution of granitic magmas. *Geol. Soc. Am. Bull.* **1988**, *100*, 1886–1897. https://doi.org/10.1130/spe253-p387.
39. Rubatto, D. Zircon: The metamorphic mineral. *Rev. Mineral. Geochem.* **2017**, *83*, 261–295. https://doi.org/10.2138/rmg.2017.83.9.
40. Grimes, C.B.; John, B.E.; Kelemen, P.B.; Mazdab, F.K.; Wooden, J.L.; Cheadle, M.J.; Hanghøj, K.; Schwartz, J.J. Trace element chemistry of zircons from oceanic crust: A method for distinguishing detrital zircon provenance. *Geology* **2007**, *35*, 643–646. https://doi.org/10.1130/G23603A.1.
41. Liu, F.; Robinson, P.T.; Gerdes, A.; Xue, H.; Liu, P.; Liou, J.G. Zircon U–Pb ages, REE concentrations and Hf isotope compositions of granitic leucosome and pegmatite from the north Sulu UHP terrane in China: Constraints on the timing and nature of partial melting. *Lithos* **2010**, *117*, 247–268. https://doi.org/10.1016/j.lithos.2010.03.002.
42. Skublov, S.G.; Berezin, A.V.; Li, X.H.; Li, Q.L.; Salimgaraeva, L.I.; Travin, V.V.; Rezvukhin, D.I. Zircons from a pegmatite cutting eclogite (Gridino, Belomorian Mobile Belt): U-Pb-O and trace element constraints on eclogite metamorphism and fluid activity. *Geosciences* **2020**, *10*, 197. https://doi.org/10.3390/geosciences10050197.
43. Soman, A.; Geisler, T.; Tomaschek, F.; Grange, M.; Berndt, J. Alteration of crystalline zircon solid solutions: A case study on zircon from an alkaline pegmatite from Zomba–Malosa, Malawi. *Contrib. Mineral. Petrol.* **2010**, *160*, 909–930. https://doi.org/10.1007/s00410-010-0514-2.
44. Černý, P.T.; Ercit S. The classification of granitic pegmatites revisited. *Can. Mineral.* **2005**, *43*, 2005–2026. https://doi.org/10.2113/gscanmin.43.6.2005.
45. Kirkland, C.L.; Smithies, R.H.; Taylor, R.J.M.; Evans, N.; McDonald, B. Zircon Th/U ratios in magmatic environs. *Lithos* **2015**, *212*, 397–414. https://doi.org/10.1016/j.lithos.2014.11.021.
46. Yakymchuk, C.; Kirkland, C. L.; Clark, C. Th/U ratios in metamorphic zircon. *J. Metamorph. Geol.* **2018**, *36*, 715–737. https://doi.org/10.1111 /jmg.12307.
47. Young, D.J.; Kylander-Clark, A.R.C. Does continental crust transform during eclogite facies metamorphism? *J. Metamorph. Geol.* **2015**, *33*, 331–357. https://doi.org/10.1111/jmg.12123.
48. Berezin, A.V.; Skublov, S.G.; Marin, Y.B.; Mel'nik, A.E.; Bogomolov, E.S. New occurrence of eclogite in the Belomorian Mobile Belt: Geology, metamorphic conditions, and isotope age. *In Doklady Earth Sciences, Springer Nature BV*. **2013**, *448*, 43. https://doi.org/10.1134/S1028334X13010029389.
49. Shatsky, V.S.; Sitnikova, E.S.; Tomilenko, A.A.; Ragozin, A.L.; Koz'menko, O.A.; Jagoutz, E. Eclogite–gneiss complex of the Muya block (East Siberia): Age, mineralogy, geochemistry, and petrology. *Russ. Geol. Geophys.* **2012**, *53*, 501–521. https://doi.org/10.1016/j.rgg.2012.04.001.
50. Palin, R.M.; Reuber, G.S.; White, R.W.; Kaus, B. J.; Weller, O. M. Subduction metamorphism in the Himalayan ultrahigh-pressure Tso Morari massif: An integrated geodynamic and petrological modelling approach. *Earth Planet. Sci. Lett.* **2017**, *467*, 108–119. https://doi.org/10.1016/j.epsl.2017.03.029.
51. Schorn, S. Self-induced incipient 'eclogitization' of metagranitoids at closed-system conditions. *J. Metamorph. Geol.* **2022**, *40*, 1271–1290. https://doi.org/10.1111/jmg.12665.
52. Proyer, A. The preservation of high-pressure rocks during exhumation: Metagranites and metapelites. *Lithos*. **2003,** *70*, 183–194. https://doi.org/10.1016/S0024-4937(03)00098-7.
53. Udoratina, O.V.; Kulikova, K.V.; Shuyskiy, A.S.; Soboleva, A.A.; Andreichev, V.L.; Golubeva, I.I.; Kapitanova, V.A. Granitoid magmatism in the north of the Urals: U–Pb age, evolution, sources. *Geodyn. Tectonophys.* **2021**, *12*, 287–309. https://doi.org/10.5800/GT2021-12-2-0525.